



CHORUS

This is the accepted manuscript made available via CHORUS. The article has been published as:

Impact of organic molecule rotation on the optoelectronic properties of hybrid halide perovskites

Qiaoling Xu, Alessandro Stroppa, Jian Lv, Xingang Zhao, Dongwen Yang, Koushik Biswas, and Lijun Zhang

Phys. Rev. Materials **3**, 125401 — Published 3 December 2019

DOI: [10.1103/PhysRevMaterials.3.125401](https://doi.org/10.1103/PhysRevMaterials.3.125401)

Impact of organic molecule rotation on the optoelectronic properties of hybrid halide perovskites

Qiaoling Xu,^{1,2} Alessandro Stroppa,³ Jian Lv,¹ Xingang Zhao,¹ Dongwen Yang,¹ Koushik Biswas,⁴ and Lijun Zhang^{1,*}

¹Key Laboratory of Automobile Materials of MOE,

and School of Materials Science and Engineering, Jilin University, Changchun 130012, China

²Center for Computational Sciences, Sichuan Normal University, Chengdu, 610068, China

³CNR-SPIN, c/o Dip.to di Scienze Fisiche e Chimiche - Via Vetoio - 67100 - Coppito (AQ), Italy

⁴Department of Chemistry and Physics, Arkansas State University, State University, AR 72467, USA

(Dated: August 27, 2019)

The importance of organic molecular cation orientation and interaction with surrounding inorganic framework in the optoelectronic hybrid halide perovskites is a topic of considerable interest. To that end, we study the effect of organic molecule rotations on the properties of such hybrid semiconductors using swarm intelligence based structure prediction method combined with *ab initio* density functional calculations. Adopting the cubic phases of APbI₃ (A = CH₃NH₃(MA), CHNH₂NH₂(FA) and CH₃CH₂NH₃(EA)), we determine the energetically stable/metastable configurations of organic molecules inside the quasi-cubic perovskite cages. Different cation orientations result in up to ~250 meV/formula changes in the material free energy, reflecting the complex energy landscape of these hybrid materials containing dynamically rotating organic components. Notably, the [012] orientation of MA is found to give the most stable structure of MAPbI₃, while the conventional [001], [011] or [111] directions remain slightly higher in energy. Molecular orientations clearly influence the fundamental electronic band gap and also modify the magnitude of Rashba-type energy band splitting resulting in indirect gap behavior. However, the dielectric screening remains large for all orientations thus creating weakly bound excitons. Based on the analysis of many organic molecule configurations obtained through structure search technique, our results provide insightful understanding on the effects of organic molecule rotation on optoelectronic properties and carrier dynamics of hybrid halide perovskites.

PACS numbers: 31.15.E-; 71.15.Mb, 71.20.Nr, 72.40.+w, 73.50.Pz, 78.20.-e

I. INTRODUCTION

Photovoltaic (PV) devices based on hybrid lead-halide perovskites have quickly reached a certified power conversion efficiency of above 25%¹, rivaling that of the more traditional and widely investigated solar cell materials. Great attention has been considered for their fundamental properties that impact PV performances^{2,3}. These materials feature unique set of characteristics: tunable band gaps⁴, strong optical absorption^{5,6}, long carrier lifetime and diffusion lengths⁷⁻¹⁰, weak exciton binding energy¹¹⁻²⁴ and tolerance towards deep defects.²⁵⁻²⁸. The underlying physical mechanisms responsible for these advantageous properties continue to be a topic of investigation.

The orientation of the organic dipoles embedded within the cubo-octahedral cavity formed by the lead-halide octahedral network, represent a subtle condition in the geometrical configuration of hybrid perovskites. It is believed that hybrid perovskites are dynamical materials where the dipole orientations and concerted octahedral tilting introduce a level of disorder in the crystals. Although X-ray diffraction can distinguish the different crystalline phases of hybrid perovskites, it does not provide full information on the position and orientation of the organic molecules relative to the inorganic framework. There is, however, additional exper-

imental evidence that strongly favor orientational disorder among the organic cations²⁹⁻⁴⁰. Many computational studies have also addressed rotational motion, reorientation dynamics and their effects on the electronic properties^{30,32,33,41-45}. It has been suggested that the molecules may behave as nearly free rotors in the room-temperature tetragonal and high-temperature cubic phases of MAPbI₃^{46,47}. Even though the organic cations in cubic MAPbI₃ are highly disordered, their orientations can still be considered discrete. Onoda-Yamamuro *et al* proposed three models based on thermal analysis which describes discrete molecular orientations with the C-N axis directed towards the face [100], edge [110] and corner [111] of cubic MAPbI₃²⁹. Other reports also suggested preferential molecular orientations in cubic^{25,44,46,48-55} and tetragonal phase hybrid perovskites⁵⁰. Quasielastic neutron scattering measurements by Leguy *et al* showed hopping MA rotations where the organic dipoles jump between preferential orientations on a timescale of several picoseconds, ruling out the possibility of free rotations at temperatures below 370 K³⁷. At temperatures relevant for solar cell operation one could envisage multiple local minima in the ground state potential energy surface of hybrid perovskites characterized by different molecular orientations resulting in local symmetry breaking^{56,57}, instantaneous structure having implications on the electronic properties⁵⁷. Thus, what is

observed experimentally is only an average crystal geometry while the material continually distorts, consequent to the organic rotations and associated tilting of the Pb-I octahedra.

While it is known that the molecular states are not directly involved in the band edges⁵⁸, the role of molecular rotations seem to have a strong influence on the inorganic framework, indirectly affecting the electronic and optical response of hybrid perovskites^{43,49,53}. Preferential organic orientations locally perturb the Pb-I lattice causing octahedral distortions, leading to variations in the band gap and carrier effective mass, which eventually control charge carrier dynamics and recombination^{4,59–61}. A comprehensive look at molecular orientations in hybrid perovskites and how they impact electronic properties is thus very important. This will be the focus of the current study.

To study the importance of molecular orientations in hybrid perovskites, we have implemented first-principles particle swarm optimization (PSO) structure search calculations including van der Waals dispersion (vdW) correction. **Though both the previous molecular dynamics (MD) calculations^{30,38,41–43,62,63} and our work can evaluate the rotation energy barriers of organic molecules, our work may add new aspects: First, the combination of PSO with first-principles calculations allows us to explore numerous structures in the energy landscape of hybrid perovskites. The PSO in principle can overcome much larger barriers in the energy landscape more efficiently than the MD approach to obtain possible new orientation of organic molecules. Secondly, thousands of static electronic structure calculations from structure searches enable us to investigate the extent to which the free energy and materials properties related to optoelectronic application are affected by the molecular reorientations coupled with octahedral tilting.** For this study, cubic phase of APbI₃ with three different organic cations (A= CH₃NH₃(MA), CHNH₂NH₂(FA) and CH₃CH₂NH₃(EA)) are chosen. The generated structures and their electronic properties reveal interesting patterns in the evolution of band gap (E_g), Rashba band splitting, effective mass and exciton binding energy. The results indicate variability among these properties, thus emphasizing the important role of the size and orientation of organic molecules.

II. COMPUTATIONAL DETAILS

The preferable orientations of MA, FA, and EA within the PbI₃ framework is explored via particle swarm optimization (PSO) algorithm as implemented in the CALYPSO code^{64,65}. For instance, the identified stable and metastable structures obtained from a population of candidate solutions of MAPbI₃ are shown in Fig. 1.

For the generation of the initial structures evolved we considered the cubic PbI₃ framework, fixing the center of mass of MA, FA, and EA molecules at the ideal A-

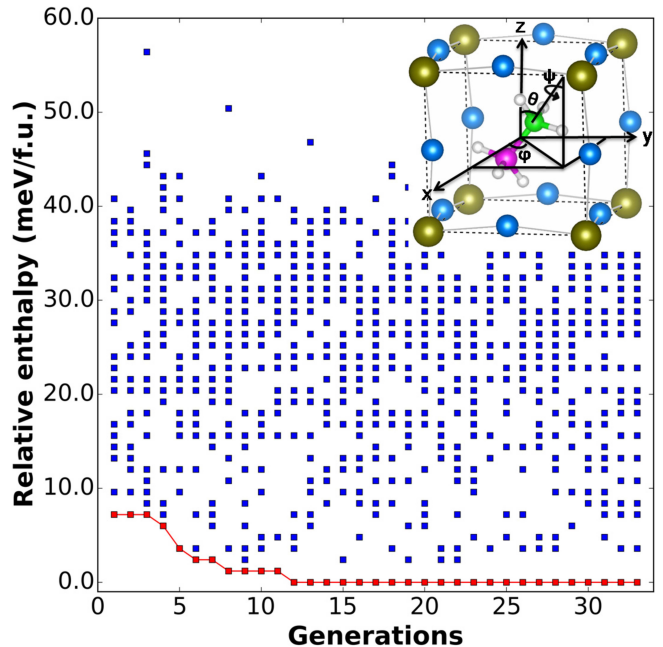


FIG. 1: (color online) Relative energy of predicted configurations as function of generation for the MAPbI₃. The inset show three freedom degrees of rotation (polar angle (θ), azimuthal angle (ϕ), spinning angle (ψ)) which are evolved by the PSO in the molecule MA embedded the framework of PbI₃

site and allowing them to rotate freely about C-N or C-C axes as appropriate for the respective cases. The rotation of the organic cations is determined by three degrees of freedom: polar angle (θ), azimuthal angle (ϕ) and spinning angle (ψ), as shown Fig. 1 and Fig. S1. Keeping the same cubic symmetry among the three lead halide perovskites allow systematic comparison as the internal geometry and corresponding electronic structure evolve due to organic cation rotations. We note that FAPbI₃ and MAPbI₃ have been experimentally reported to adopt a cubic structure at 298 K and above 327 K, respectively^{66,67}. We constrain EAPbI₃ in the same structure, although this system was recently reported in the orthorhombic phase having chain like features with intervening EAs⁶⁸.

For structure evolution, PSO is used, as a global optimization algorithm, which is inspired by the social behavior of birds flocking or fish schooling. It can be seen as a distributed behavior algorithm that performs multi-dimensional search. In practice, a candidate structure in the configurational space is regarded as a particle, and a set of individual particles is called a population/generation. Each particle explores the search space via a velocity vector which is affected by both its personal best experience and the best position found by the population thus far. During the process of evolution, the

structures satisfy the following equations:

$$x_{ij}^{t+1} = x_{ij}^t + v_{ij}^{t+1} \quad (1)$$

$$v_{ij}^{t+1} = \omega v_{ij}^t + c_1 r_1 (pbest_{ij}^t - x_{ij}^t) + c_2 r_2 (gbest_{ij}^t - x_{ij}^t) \quad (2)$$

where i is a structure regarded as a particle in the search space and $j \in \{\theta, \phi, \psi\}$. Eq. (1) is used to update the positions of the particles. The new position of each individual i at the j th dimension is calculated based on its previous location (x_{ij}^t) before optimization and its new velocity (v_{ij}^{t+1}). The latter depends on previous velocity (v_{ij}^t), current location ($pbest_{ij}^t$) with an achieved best fitness of lowest enthalpy of the particle, and the best global fitness value for the entire population (swarm) ($gbest_{ij}^t$), according to Eq. (2). ω denotes the inertia weight and controls the momentum of the particle.

Structure optimization is conducted within the density functional theory (DFT) using plane-wave pseudopotential method implemented in the Vienna Ab-initio Simulation Package (VASP)⁶⁹. Electron-ion interaction is described using projector augmented-wave (PAW) pseudopotentials⁷⁰. The $2s^2 2p^2$ states of C, $2s^2 2p^3$ of N, $2s^2 2p^4$ of O, $1s$ of H, $6s^2 6p^2$ of Pb, and $5s^2 5p^5$ of I are included as valence electrons. We use Perdew, Burke and Ernzerhof (PBE)^{71,72} as the exchange correction functional. An energy cutoff of 470 eV and the mesh of k-points of $6 \times 6 \times 6$ (MAPbI₃) and $5 \times 5 \times 5$ (FAPbI₃ and EAPbI₃) are used for geometry optimization and electronic structure calculations. **Convergence tests indicate that the total energy converges at an accuracy of less than 0.1 meV/atom with respect to cutoff energy, and at an accuracy of 0.2 meV/atom with respect to the k-point sampling (Fig. S2).** Long-range dispersion interactions, which play an important role^{53,73–75} on organic cation orientation and structure determination, are considered in this work. We compared the equilibrium lattice parameters of MAPbI₃ in cubic phase (see the Table S1) and found that both optB86b and optB88b van der Waals (vdWs) functionals⁷⁶ provide better agreement, within about 0.3% of experimental values⁴⁶. The optB86b vdW functional is adopted for all subsequent calculations. In order to constrain the cubic symmetry, all structures are optimized by fixing cell shape ($a=b=c$), while relaxing their volumes and internal coordinates.

For band gap calculations of the most stable configurations with favored molecular orientations, we used hybrid functional (HSE)⁷⁷ with adjustable Fock exchange (given by mixing parameter $\alpha=55\%$)⁷⁸ and including spin-orbit coupling (SOC). The calculated results show reasonable agreement with available experimental data as shown below. We also found that the band gaps from the HSE+SOC approach are very close to the DFT-PBE derived values, as demonstrated in Fig. 2. This has been reported in literature²⁵, i.e., neglecting the SOC effect leads to fortuitous agreement between calculated

DFT-PBE and experimental band gaps of hybrid halide perovskites. Thus, we used the DFT-PBE approach to obtain fairly accurate band gap estimates of thousands of searched structures caused by reorientation of the organic molecules. We used the DFT-PBE approach, including SOC, to calculate the Rashba-type splitting near the band edges, which is caused by broken inversion symmetry associated with molecular orientations.

We also use the BoltzTraP code⁷⁹ to calculate carrier effective mass (m^*) tensors with a dense k-point grid of $10 \times 10 \times 10$ and unified carrier concentration of $1.0 \times 10^{18} \text{ cm}^{-3}$ at temperature of 300 K. **We calculated carrier effective masses of stable configurations with the favored molecular orientations by using the DFT-PBE approach with and without the SOC effect, as shown in supplementary Table S2. For the three hybrid perovskites, the hole effective masses remain almost unaffected by the SOC, while the electron masses were uniformly overestimated by the DFT-PBE approach without the SOC. This is expected since the SOC mainly affects the Pb- p orbitals dominating conduction bands, but has no impact on the valence bands derived from Pb- s states (where the relativistic Darwin effect causes the energy level upshift). For thousands of searched structures caused by reorientation of organic molecules, our goal is to explore the extent to which the carrier effective masses are affected by the molecular reorientations coupled with octahedral tilting. Considering the computational cost of the effective mass calculations needing dense k-point grid when the SOC is included, we employed the DFT-PBE approach w/o SOC for such calculations. As such, we note that our calculated effective masses of conducting electrons are clearly overestimated.** Then, an estimation of the binding energy (E_B) of the hydrogenic Wannier-Mott exciton is made, using $E_B = \mu R_y / m_0 \epsilon_\infty^2$, where μ is reduced carrier effective mass ($1/\mu = 1/m_e^* + 1/m_h^*$), ϵ_∞ is the calculated high-frequency dielectric constant obtained by perturbation theory within PBE and R_y is the atomic Rydberg energy.

III. RESULTS AND DISCUSSION

As shown in Fig. 1 and Fig. S1, different cation orientations result in up to ~ 60 meV/formula for MAPbI₃, ~ 150 meV/formula for FAPbI₃ and ~ 250 meV/formula for EAPbI₃ changes in the ground-state total energy. This reflects the complex energy landscape of these hybrid materials containing dynamically rotating organic components. Fig. 2(a, b, c) shows favored molecular orientation in the predicted stable configurations of the three compounds: MAPbI₃, FAPbI₃, and EAPbI₃ (structural details are summarized in Table S3). Corresponding lattice parameters are 6.310 Å (experiment: 6.328 Å⁶⁶), 6.370 Å (experiment: 6.362 Å⁶⁷), and 6.418 Å for MAPbI₃, FAPbI₃, and EAPbI₃, consistent with the increasing size of the organic cations MA⁺, EA⁺, FA⁺. The arrows in Fig. 2 represent molecular dipole

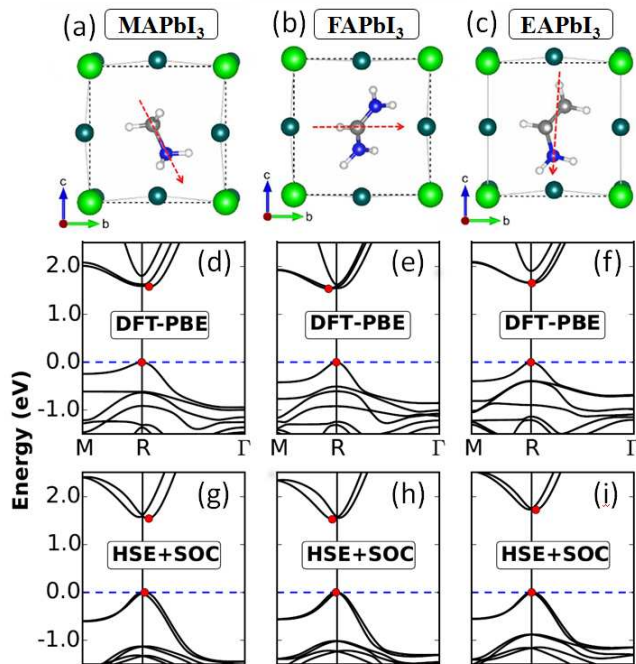


FIG. 2: (color online) The predicted stable structures and calculated corresponding band structures using PBE and HSE (with adjustable Fock exchange, given by mixing parameter $\alpha=55\%$)+SOC functional respectively for MAPbI₃ (a, d, g), FAPbI₃ (b, e, h) and EAPbI₃ (c, f, i). Note that the MA directed to the orientation [012].

moments. It is interesting to note that the C-N axis of MA⁺ is directed along [012] with *Pm* symmetry in the predicted lowest energy configuration of MAPbI₃ cubic unit cell; deviating from the conventional [100],^{44,49–52} [110],^{48,53} and [111] directions^{25,54,55}) which are commonly cited in the literature. The calculated total energies of [110], [001] and [111] orientations are higher than that of [012] by 16, 26, 45 meV/formula unit, respectively. In case of FAPbI₃, it has been suggested that the C-H bond of FA⁺ is directed towards a cube face [100], thus minimizing the (C-H)⋯I interactions while the C-Ns are oriented in a way that allow (N-H)⋯I hydrogen bonds⁶⁷. Our structure search predicts a different FAPbI₃ ground state where the N-CH-N part of FA lies approximately within the (111) plane, distinct from the FA lying in the (200) plane in Ref. 67. We find this configuration of FAPbI₃ to be more stable, by about 124 meV/formula unit, compared to the one where the C-H bond is directed along [100]. The preferred molecular orientations in MAPbI₃ and FAPbI₃ predicted by the structure search approach potentially means increased hydrogen bonding ((N-H)⋯I bonds) in the distorted, pseudocubic hosts - emphasizing the interplay between organic motifs and inorganic framework in these dynamical materials. Relatively small energy differences between specific configurations also imply that the molecules may be rotationally mobile at room temperature i.e., their ori-

entations continue to evolve due to rotor-like or tumbling motion, without the possibility of long range ferroelectric ordering.

The electronic band structures of MAPbI₃, FAPbI₃, and EAPbI₃ stable configurations are shown in Fig. 2. As is well-known in the case of hybrid perovskites, neglecting spin-orbit effects leads to fortuitous agreement between calculated PBE band gaps (E_g) and experimental values. Nevertheless, **it provides reasonable estimates as evident from the comparison with the results calculated by the HSE+SOC functional with adjustable Fock exchange (given by mixing parameter $\alpha=55\%$), shown in Fig. 2.** However, band splitting and band-edge position relative to the core levels are more accurately described when spin-orbit coupling and nonlocal exchange interaction is included as in the case of HSE+SOC. The calculated HSE+SOC gaps are 1.54, 1.52, 1.72 eV for MAPbI₃, FAPbI₃, and EAPbI₃ following the trend: $E_g(\text{FA}) < E_g(\text{MA}) < E_g(\text{EA})$, which is in reasonable agreement with available experimental results: $\sim 1.5\text{-}1.7$ eV in MAPbI₃^{80–87} and $1.43\text{-}1.48$ eV in FAPbI₃^{60,88–90}. All structures show an indirect band gap near the high symmetry R point as indicated in Fig. 2.

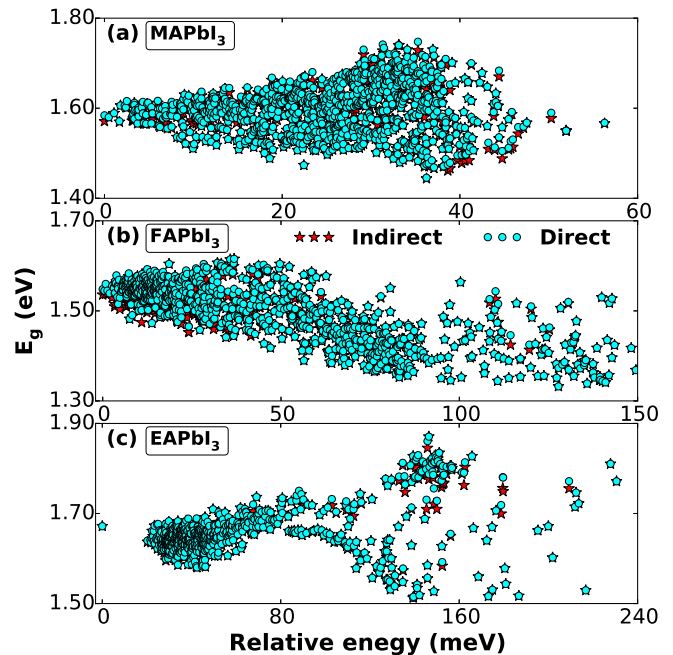


FIG. 3: (color online) Calculated band gaps using DFT-PBE functional for the MAPbI₃ (a), FAPbI₃ (b), EAPbI₃ (c) as function of the energy range when the molecules are evolved to rotate in the space.

Next, we describe the 'dynamical band gap' behavior caused by molecular reorientations coupled with octahedral tilting as obtained from our search. For example, in case of MAPbI₃ the HSE+SOC calculated band gap changes from 1.54 eV in the preferred [012] organic orientation (most stable structure) to about 1.47 eV when

cations are directed along [111]. Fig. 3 shows band gap variations of the searched structures in all three compounds **caused by reorientation of the differently sized organic cations and corresponding distortions of the Pb-I octahedral framework**⁹¹. The presented gap values are based on PBE functional without spin-orbit coupling and plotted as a function of relative energy w.r.t the most stable structure. In a previous study, Mosconi et al investigated the dynamics of organic rotations, observing that the Highest Occupied Molecular Orbital (HOMO) level varied within ~ 0.5 eV in cubic MAPbI₃³⁰. They also studied FA molecular dynamics in cubic FAPbI₃, estimating in this case band gap changes ranging within 0.2 eV⁴³. The plot in Fig. 3 shows a similar range of band gap values obtained through the structure evolution process. It is clear that the molecular orientation can strongly influence the band gap of the hybrid perovskites by affecting the I-Pb-I inorganic framework which take part in the frontier orbitals. The PSO approach employed in our current study can efficiently overcome larger barriers in the potential energy landscape of these perovskites, and consequently provide an accurate estimate of band gap variation obtainable via molecular rotation and concerted octahedral tilting. Our results indicate band gap values approximately ranging between 1.5-1.7 eV in MAPbI₃, 1.3-1.6 eV in FAPbI₃, and 1.5-1.9 eV in EAPbI₃.

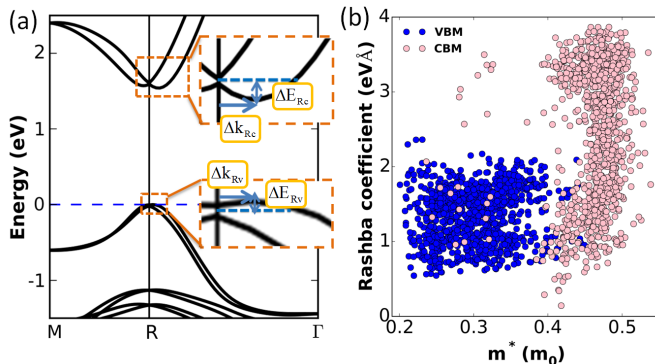


FIG. 4: (color online). (a) The illustration of the rashba splitting for the ground-state of MAPbI₃ structures in the VBM and CBM and (b) calculated rashba coefficient with the energies of no more than 60 meV/f.u. higher than the ground-state for the MAPbI₃ structures in the VBM ($\alpha_v = 2 \Delta E_{Rv} / \Delta k_{Rv}$) and CBM ($\alpha_c = 2 \Delta E_{Rc} / \Delta k_{Rc}$) along the high symmetry direction of the Brillouin zone R (0.5, 0.5, 0.5) \rightarrow Γ (0.0, 0.0, 0.0) as function of the effective mass. **The calculations were done by using the DFT-PBE approach, including SOC.**

Another impact of molecular rotation is small variations in k-space splitting (Rashba-type splitting) near band edge that causes indirect gaps. This effect, reported in similar hybrid perovskites,⁹²⁻⁹⁶ is a consequence of inversion symmetry breaking. This feature available among the hybrid materials may help suppress exciton formation and delay charge carrier recombina-

tion, which is essential for solar cell application⁵³. All-inorganic perovskite such as CsPbBr₃ have direct band gap (~ 2.3 eV), and known to luminesce with green excitonic emission in bulk or nanocrystalline forms^{97,98}. The strength of Rashba-type splitting among hybrid perovskites can be approximately quantified via the Rashba parameter, $\alpha = 2\Delta E_R / \Delta k_R$,⁹⁹ where Δk is the momentum offset in k-space of the conduction band minimum (CBM) or valence band maximum (VBM) w.r.t the high symmetry k-point. It is shown for MAPbI₃ along R- Γ in Fig. 4(a). ΔE_R is the corresponding energy difference. The estimated α values of VBM/CBM in our predicted stable configurations of MAPbI₃, FAPbI₃ and EAPbI₃ are 1.16/2.64, 0.59/0.97 and 0.84/1.81 eVÅ, respectively. It is clear that Rashba parameters of the CBM are higher than those of the VBM in all three compounds, attributable to the spin-split Pb 6p orbitals that make up the conduction edge. Fig. 4(b) depicts the Rashba parameters given as a function of calculated electron or hole effective mass for the different MA orientations obtained in the structure search of MAPbI₃. It indicates a wide range of achievable values of α , greater than those predicted earlier¹⁰⁰, approaching 4 eVÅ in the CBM and upto 2 eVÅ in the VBM. Hence, Rashba-type spin splitting caused by molecular reorientations may be one of the key features that help reduce charge carrier recombination and improve efficiency of hybrid perovskite-based solar cells^{92,93,95}.

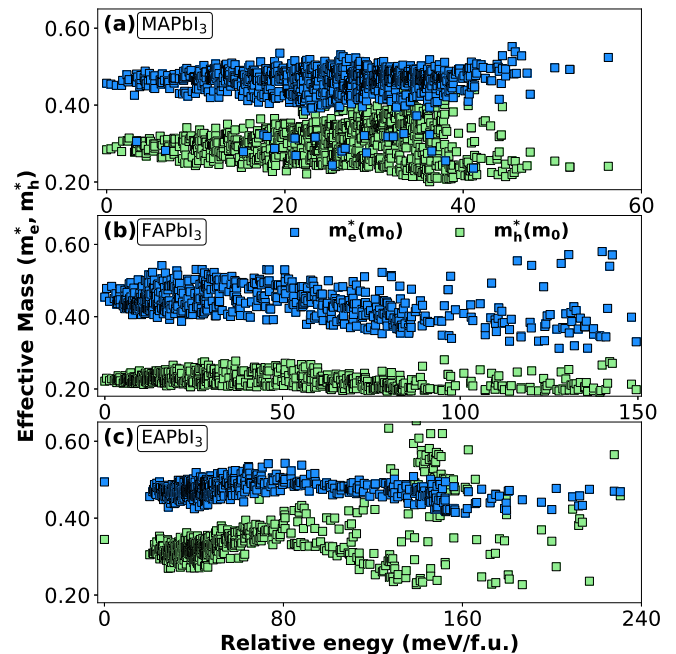


FIG. 5: (color online) Calculated effective mass of electron and hole **using DFT-PBE functional** for the MAPbI₃ (a), FAPbI₃ (b), EAPbI₃ (c) as function of the energy range with the evolution of the θ , ϕ and ψ angles by rotating the molecules.

Effective mass (m^*) tensors that relate directly to car-

rier’s electrical conductivity are calculated using the PBE functional. Carrier effective masses of various structures as a function of relative energy w.r.t the most stable configuration are shown in Fig. 5. The electron masses (m_e^*) approximately range 0.4-0.6 m_0 (m_0 being the electron rest mass) in all three compounds, and that of holes (m_h^*) between 0.2-0.4 m_0 in MAPbI₃, 0.2-0.3 m_0 in FAPbI₃, and 0.3-0.4 m_0 in EAPbI₃. The results underscore variable m^* as the molecules are allowed to rotate within the Pb-I framework. Specific values of different MAPbI₃ structures along k_x , k_y and k_z directions are shown in Fig. S3. **The most stable configurations of MAPbI₃, FAPbI₃ and EAPbI₃ yield values of 0.29(0.26), 0.22(0.20) and 0.34(0.32) m_0 for the holes and 0.46(0.22), 0.47(0.27), 0.51(0.38) m_0 for electrons without(with) the SOC effect, respectively. For the three hybrid perovskites, the hole effective masses remain almost unaffected by the SOC, while the electron masses were uniformly overestimated by the DFT-PBE approach without the SOC. This is expected since the SOC mainly affects Pb- p orbitals dominating the conduction bands, but has no impact on the valence bands derived from Pb- s (where the relativistic Darwin effect causes the energy level upshift). The estimated effective mass of MAPbI₃ is in reasonable agreement with reported m_e^* of 0.35 m_0 and m_h^* of 0.31 m_0 ¹⁰¹. Low electron and hole effective masses due to the dispersive band edges contribute to the good, ambipolar electrical conductivity observed in experiment and theory calculations^{7,55}.**

A notable aspect of Figs. 3 and 5 is the horizontal scale which represents the energy difference between the most stable and the least stable molecular orientations among the metastable (local minima) structures. It is about 60, 150, 240 meV/formula unit for MAPbI₃, FAPbI₃ and EAPbI₃ respectively (see Fig.S1), indicating that the larger molecules rotate less freely and more slowly in the Pb-I framework. The figures also show the corresponding distribution in band gap and effective mass values with increasing energy of the structures.

We finally turn to the dielectric properties of the pseudocubic hybrid perovskite structures generated through our PSO search. As the orientation of the organic cations are allowed to change accompanied by octahedral tilting, the static dielectric constant values remain large. Anomalously high dielectric constant separates these ionic halides from traditional III-V and II-VI compound semiconductors. To evaluate the exciton binding energy E_B within the Wannier-Mott hydrogenic model, we use the calculated high frequency dielectric constant, ϵ_∞ . **The inverse relationship between E_B and dielectric constant for hybrid perovskites has been reported previously¹⁰². Figure 6 shows E_B as a function of calculated ϵ_∞ , ranging between 50-110 meV, 50-85 meV and 70-150 meV for different metastable states of the three different hybrid perovskites. These values are in overall agreement with experimental studies that have suggested low exciton binding energy, with few reporting values as low as 2 meV in case of MAPbI₃^{11-18,20,22-24}**

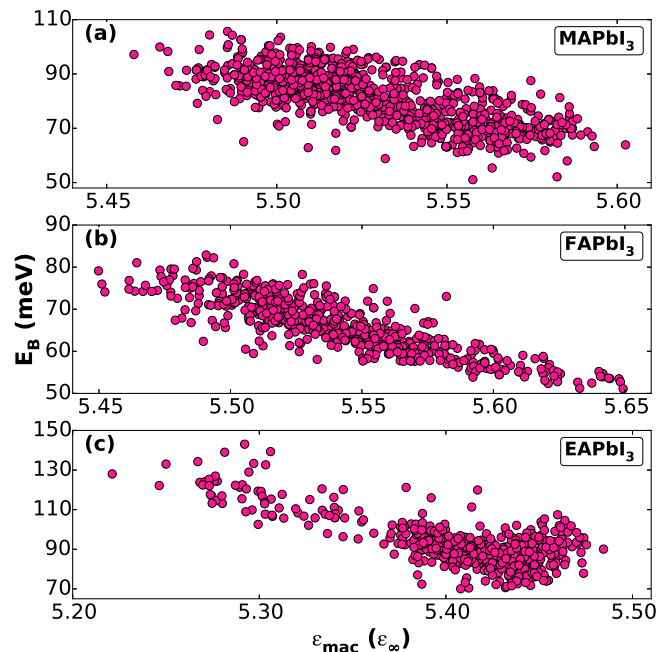


FIG. 6: (color online) Calculated exciton binding energies using DFT-PBE functional of the MAPbI₃ (a), FAPbI₃ (b), EAPbI₃ (c) respectively as function of the high-frequency limit of dielectric constant.

. As the pseudocubic structure of the hybrid perovskites constantly evolve via molecular rotations, the exciton effective mass (not shown) and binding energy values remain consistently low. Considering that the exciton radii are large, equal or greater than the lattice constant, the electron-hole screened interaction is impacted by molecular rotations that cause local lattice polarization. We, thus, emphasize that reduced rate of bimolecular recombination among hybrid perovskites is a consequence of strong screening of electron-hole pairs by large static dielectric constant and low exciton binding energy; a consequence of lattice polarization caused by molecular rotations and induced octahedral tilting.

Finally, to simulate different equivalent alignments of organic molecules, we have performed the calculations with the $2 \times 2 \times 2$ supercell of MAPbI₃, where for selected orientations (e.g., [001], [011], [012], [111]) the molecules are randomly aligned w.r.t. equivalent orientations. For each selected orientation, five configurations were constructed and the relevant properties such as total energy, band gap, carrier effective masses, and Rashba splitting coefficients were calculated. The results are shown in the new supplementary Fig. S4. As seen, the fact that the [012] orientation of MA leads to the energetically most favorable structure is valid for all the configurations. The other properties such as band gap, carrier effective masses, Rashba splitting coefficients show variation within a reasonably small range. These results indicate that the main findings discussed by using the unit cubic perovskite cell indeed are maintained when

the larger supercell with different equivalent molecular orientations are used. It should be pointed out that we are not claiming a perfect correlation or alignment is expected throughout the entire volume of these hybrid perovskites. Rather, it emphasizes a local microstructure is possible in these dynamical materials. The bulk crystal's response is an average over such microstructures which consist of preferred molecular orientations and corresponding octahedral distortions.

IV. CONCLUSIONS

We explored favored orientations of three different organic cations, viz., $\text{CH}_3\text{NH}_3(\text{MA})$, $\text{CHNH}_2\text{NH}_2(\text{FA})$ and $\text{CH}_3\text{CH}_2\text{NH}_3(\text{EA})$ inside the polyhedral cages of pseudocubic lead-halide perovskites and its impact on the electronic structure. Local metastable structures are searched by the particle swarm optimization algorithm combined with the first principles DFT calculations. In case of MAPb_3 , we find the [012] orientation of the MA cation to be most stable, separate from the commonly known [100], [110], and [111] orientations discussed in the literature. This study highlights the complex energy landscape formed by the metastable structures among hybrid preovskites and the effect of varying molecular orientations on their dynamical gap behavior, and Rashba splitting - both of which are connected to carrier generation and recombination that impact device performance. The dichotomy between predicted low effective mass of charge carriers and low-to-moderate carrier mobility has been a subject of debate. Deformation potential scattering by acoustic phonons, possibility of large polarons, even strongly bound small polarons have been suggested

as possible reasons for moderate mobility^{103–107}. Our previous works described the possibility of electrostatic polarization caused by molecular reorientation that is indicative of long range coupling, creating shallow trap-like states that bind charge carriers within a few kT of the CBM or VBM¹⁰⁸. Current structure search indicates a similar phenomenon where molecular reorientations via three rotational degrees of freedom give rise to pseudocubic metastable structures, all of whom have low carrier effective mass. This finding is consistent with the view that at room or higher temperatures a global ground state structure may be elusive as a result of organic rotation and octahedral tilting, whose phonon cloud "protect" the charge carrier by enhancing both its mass and lifetime. The crystal, however, maintains its average geometry. Additionally, we find that the exciton binding energy values remain consistently low among all searched structures. Thus, large exciton radius and strong screening may be the hallmarks of the hybrid perovskites that lead to reduced bimolecular pairing and efficient collection of photo-generated charge carriers.

V. ACKNOWLEDGEMENT

The work at Jilin University is supported by the National Natural Science Foundation of China (Grant No. 61722403 and 11674121), Jilin Province Science and Technology Development Program (Grant No. 20190201016JC) and Program for Jilin University Science and Technology Innovative Research Team. Calculations were performed in part at the high performance computing center of Jilin University.

* Electronic address: lijun_zhang@jlu.edu.cn

¹ *Best research-cell efficiencies*, <https://www.nrel.gov/pv/assets/pdfs/pv-efficiency-chart.20190103.pdf>.

² M. M. Lee, J. Teuscher, T. Miyasaka, T. N. Murakami, and H. J. Snaith, *Science* **338**, 643 (2012).

³ Q. Xu, D. Yang, J. Lv, Y.-Y. Sun, and L. Zhang, *Small Methods* **2**, 1700316 (2018).

⁴ M. R. Filip, G. E. Eperon, H. J. Snaith, and F. Giustino, *Nat. Commun.* **5**, 5757 (2014).

⁵ A. Kojima, K. Teshima, Y. Shirai, and T. Miyasaka, *J. Am. Chem. Soc.* **131**, 6050 (2009).

⁶ S. De Wolf, J. Holovsky, S.-J. Moon, P. Löper, B. Niesen, M. Ledinsky, F.-J. Haug, J.-H. Yum, and C. Ballif, *J. Phys. Chem. Lett.* **5**, 1035 (2014).

⁷ S. D. Stranks, G. E. Eperon, G. Grancini, C. Menelaou, M. J. P. Alcocer, T. Leijtens, L. M. Herz, A. Petrozza, and H. J. Snaith, *Science* **342**, 341 (2013).

⁸ G. Xing, N. Mathews, S. Sun, S. S. Lim, Y. M. Lam, M. Grätzel, S. Mhaisalkar, and T. C. Sum, *Science* **342**, 344 (2013).

⁹ D. Yang, W. Ming, H. Shi, L. Zhang, and M.-H. Du, *Chem. Mater.* **28**, 4349 (2016).

¹⁰ Y. Wang, Y. Zhang, P. Zhang, and W. Zhang, *Phys. Chem. Chem. Phys.* **17**, 11516 (2015).

¹¹ A. Miyata, A. Mitoglu, P. Plochocka, O. Portugall, J. T.-W. Wang, S. D. Stranks, H. J. Snaith, and R. J. Nicholas, *Nature Phys.* **11**, 582 (2015).

¹² Y. Yamada, T. Nakamura, M. Endo, A. Wakamiya, and Y. Kanemitsu, *IEEE J. Photovolt.* **5**, 401 (2015).

¹³ K. Tanaka, T. Takahashi, T. Ban, T. Kondo, K. Uchida, and N. Miura, *Solid State Commun.* **127**, 619 (2003).

¹⁴ V. D'Innocenzo, G. Grancini, M. J. Alcocer, A. R. S. Kandada, S. D. Stranks, M. M. Lee, G. Lanzani, H. J. Snaith, and A. Petrozza, *Nat. Commun.* **5**, 3586 (2014).

¹⁵ S. Sun, T. Salim, N. Mathews, M. Duchamp, C. Boothroyd, G. Xing, T. C. Sum, and Y. M. Lam, *Energy Environ. Sci.* **7**, 399 (2014).

¹⁶ M. Saba, M. Cadelano, D. Marongiu, F. Chen, V. Sarritzu, N. Sestu, C. Figus, M. Aresti, R. Piras, A. G. Lehmann, et al., *Nat. Commun.* **5**, 5049 (2014).

¹⁷ Q. Zhang, S. T. Ha, X. Liu, T. C. Sum, and Q. Xiong, *Nano Lett.* **14**, 5995 (2014).

¹⁸ T. J. Savenije, C. S. Ponseca Jr, L. Kunneman, M. Abdellah, K. Zheng, Y. Tian, Q. Zhu, S. E. Canton, I. G.

- Scheblykin, T. Pullerits, et al., *J. Phys. Chem. Lett.* **5**, 2189 (2014).
- ¹⁹ J. Song, J. Li, X. Li, L. Xu, Y. Dong, and H. Zeng, *Advanced Materials* **27**, 7162 (2015).
- ²⁰ M. Hirasawa, T. Ishihara, T. Goto, K. Uchida, and N. Miura, *Physica B: Condensed Matter* **201**, 427 (1994).
- ²¹ X. Li, Y. Wu, S. Zhang, B. Cai, Y. Gu, J. Song, and H. Zeng, *Advanced Functional Materials* **26**, 2435 (2016).
- ²² A. M. Soufiani, Y. Zhuo, T. Young, A. Surrente, A. R. Pascoe, K. Galkowski, M. Abdi-Jalebi, R. Brenes, J. Urban, N. Zhang, et al., *Energy Environ. Sci.* (2017).
- ²³ S. Tombe, G. Adam, H. Heilbrunner, D. H. Apaydin, C. Ulbricht, N. S. Sariciftci, C. J. Arendse, E. Iwuoha, and M. C. Scharber, *J. Mater. Chem. C* **5**, 1714 (2017).
- ²⁴ Z. Yang, A. Surrente, K. Galkowski, N. Bruyant, D. K. Maude, A. A. Haghighirad, H. J. Snaith, P. Plochocka-Maude, and R. J. Nicholas, *J. Phys. Chem. Lett.* **8**, 1851 (2017).
- ²⁵ W.-J. Yin, J.-H. Yang, J. Kang, Y. Yan, and S.-H. Wei, *J. Mater. Chem. A* **3**, 8926 (2015).
- ²⁶ M. H. Du, *J. Mater. Chem. A* **2**, 9091 (2014).
- ²⁷ W.-J. Yin, T. Shi, and Y. Yan, *Applied Physics Letters* **104**, 063903 (2014).
- ²⁸ W. Ming, D. Yang, T. Li, L. Zhang, and M.-H. Du, *Advanced Science* **5**, 1700662 (2018).
- ²⁹ N. Onoda-Yamamuro, T. Matsuo, and H. Suga, *J. Phys. Chem. Solids* **51**, 1383 (1990).
- ³⁰ E. Mosconi, C. Quarti, T. Ivanovska, G. Ruani, and F. De Angelis, *Phys. Chem. Chem. Phys.* **16**, 16137 (2014).
- ³¹ T. Glaser, C. Müller, M. Sendner, C. Krekeler, O. E. Semonin, T. D. Hull, O. Yaffe, J. S. Owen, W. Kowalsky, A. Pucci, et al., *J. Phys. Chem. Lett.* **6**, 2913 (2015).
- ³² A. A. Bakulin, O. Selig, H. J. Bakker, Y. L. Rezus, C. Müller, T. Glaser, R. Lovrincic, Z. Sun, Z. Chen, A. Walsh, et al., *J. Phys. Chem. Lett.* **6**, 3663 (2015).
- ³³ O. Selig, A. Sadhanala, C. Müller, R. Lovrincic, Z. Chen, Y. L. Rezus, J. M. Frost, T. L. Jansen, and A. A. Bakulin, *J. Am. Chem. Soc.* **139**, 4068 (2017).
- ³⁴ R. E. Wasylshen, O. Knop, and J. B. Macdonald, *Solid State Commun.* **56**, 581 (1985).
- ³⁵ O. Knop, R. E. Wasylshen, M. A. White, T. S. Cameron, and M. J. V. Oort, *Can. J. Chem.* **68**, 412 (1990).
- ³⁶ T. Baikie, N. S. Barrow, Y. Fang, P. J. Keenan, P. R. Slater, R. O. Piltz, M. Gutmann, S. G. Mhaisalkar, and T. J. White, *J. Mater. Chem. A* **3**, 9298 (2015).
- ³⁷ A. M. A. Leguy, J. M. Frost, A. P. McMahon, V. G. Sakai, W. Kochelmann, C. Law, X. Li, F. Foglia, A. Walsh, B. C. ÓRegan, et al., *Nat. Commun.* **6**, 7124 (2015).
- ³⁸ T. Chen, B. J. Foley, B. Ipek, M. Tyagi, J. R. Copley, C. M. Brown, J. J. Choi, and S.-H. Lee, *Phys. Chem. Chem. Phys.* **17**, 31278 (2015).
- ³⁹ K. Page, J. E. Siewenie, P. Quadrelli, and L. Malavasi, *Angew. Chem. Int. Ed.* **128**, 14532 (2016).
- ⁴⁰ I. P. Swainson, C. Stock, S. F. Parker, L. Van Eijck, M. Russina, and J. W. Taylor, *Phys. Rev. B* **92**, 100303 (2015).
- ⁴¹ A. Mattoni, A. Filippetti, M. Saba, and P. Delugas, *J. Phys. Chem. C* **119**, 17421 (2015).
- ⁴² M. A. Carignano, A. Kachmar, and J. Hutter, *J. Phys. Chem. C* **119**, 8991 (2015).
- ⁴³ C. Quarti, E. Mosconi, and F. D. Angelis, *Phys. Chem. Chem. Phys.* **17**, 9394 (2015).
- ⁴⁴ C. Quarti, E. Mosconi, and F. De Angelis, *Chem. Mater.* **26**, 6557 (2014).
- ⁴⁵ C. Quarti, E. Mosconi, J. M. Ball, V. D'Innocenzo, C. Tao, S. Pathak, H. J. Snaith, A. Petrozza, and F. De Angelis, *Energy Environ. Sci.* **9**, 155 (2016).
- ⁴⁶ A. Poglitsch and D. Weber, *J. Chem. Phys.* **87**, 6373 (1987).
- ⁴⁷ Y. Kawamura, H. Mashiyama, and K. Hasebe, *J. Phys. Soc. Jpn.* **71**, 1694 (2002).
- ⁴⁸ H. Mashiyama, Y. Kurihara, and T. Azetsu, *J. Korean Phys. Soc.* **32**, S156 (1998).
- ⁴⁹ F. Brivio, A. B. Walker, and A. Walsh, *APL Mater.* **1**, 042111 (2013).
- ⁵⁰ J. M. Frost, K. T. Butler, and A. Walsh, *APL Mater.* **2**, 081506 (2014).
- ⁵¹ J.-S. Park, S. Choi, Y. Yan, Y. Yang, J. M. Luther, S.-H. Wei, P. Parilla, and K. Zhu, *J. Phys. Chem. Lett.* **6**, 4304 (2015).
- ⁵² M. T. Weller, O. J. Weber, P. F. Henry, A. M. D. Pumpo, and T. C. Hansen, *Chem. Commun.* **51**, 4180 (2015).
- ⁵³ C. Motta, F. El-Mellouhi, S. Kais, N. Tabet, F. Alharbi, and S. Sanvito, *Nat. Commun.* **6**, 7026 (2015).
- ⁵⁴ Y. Zhou, F. Huang, Y.-B. Cheng, and A. Gray-Weale, *Phys. Chem. Chem. Phys.* **17**, 22604 (2015).
- ⁵⁵ G. Giorgi, J.-I. Fujisawa, H. Segawa, and K. Yamashita, *J. Phys. Chem. Lett.* **4**, 4213 (2013).
- ⁵⁶ O. Yaffe, *Physical Review Letters* **118**, 136001 (2017).
- ⁵⁷ A. N. Beecher, O. E. Semonin, J. M. Skelton, J. M. Frost, M. W. Terban, H. Zhai, A. Alatas, J. S. Owen, A. Walsh, and S. J. L. Billinge, *ACS Energy Lett.* **1**, 880 (2016).
- ⁵⁸ Y. Chang, C. Park, and K. Matsuishi, *J. Korean Phys. Soc.* **44**, 889 (2004).
- ⁵⁹ I. Borriello, G. Cantele, and D. Ninno, *Phys. Rev. B* **77**, 235214 (2008).
- ⁶⁰ G. E. Eperon, S. D. Stranks, C. Menelaou, M. B. Johnston, L. M. Herz, and H. J. Snaith, *Energy Environ. Sci.* **7**, 982 (2014).
- ⁶¹ N. J. Jeon, J. H. Noh, W. S. Yang, Y. C. Kim, S. Ryu, J. Seo, and S. I. Seok, *Nature* **517**, 476 (2015).
- ⁶² A. Mattoni, A. Filippetti, and C. Caddeo, *Journal of Physics: Condensed Matter* **29**, 043001 (2016).
- ⁶³ J. M. Frost and A. Walsh, *Accounts of Chemical Research* **49**, 528 (2016).
- ⁶⁴ Y. Wang, J. Lv, L. Zhu, and Y. Ma, *Phys. Rev. B* **82**, 094116 (2010).
- ⁶⁵ Y. Wang, J. Lv, L. Zhu, and Y. Ma, *Comput. Phys. Commun.* **183**, 2063 (2012).
- ⁶⁶ A. Poglitsch and D. Weber, *J. Chem. Phys.* **87**, 6373 (1987).
- ⁶⁷ M. T. Weller, O. J. Weber, J. M. Frost, and A. Walsh, *J. Phys. Chem. Lett.* **6**, 3209 (2015).
- ⁶⁸ J.-H. Im, J. Chung, S.-J. Kim, and N.-G. Park, *Nanoscale Res. Lett.* **7**, 353 (2012).
- ⁶⁹ G. Kresse and J. Furthmüller, *Phys. Rev. B* **54**, 11169 (1996).
- ⁷⁰ P. E. Blöchl, *Phys. Rev. B* **50**, 17953 (1994).
- ⁷¹ J. P. Perdew, J. A. Chevary, S. H. Vosko, K. A. Jackson, M. R. Pederson, D. J. Singh, and C. Fiolhais, *Phys. Rev. B* **46**, 6671 (1992).
- ⁷² J. P. Perdew, K. Burke, and M. Ernzerhof, *Phys. Rev. Lett.* **77**, 3865 (1996).
- ⁷³ D. A. Egger and L. Kronik, *The Journal of Physical Chemistry Letters* **5**, 2728 (2014).
- ⁷⁴ J.-H. Lee, N. C. Bristowe, P. D. Bristowe, and A. K. Cheetham, *Chemical Communications* **51**, 6434 (2015).

- ⁷⁵ Y. Wang, T. Gould, J. F. Dobson, H. Zhang, H. Yang, X. Yao, and H. Zhao, *Physical Chemistry Chemical Physics* **16**, 1424 (2013).
- ⁷⁶ J. Klimeš, D. R. Bowler, and A. Michaelides, *J. Phys. Condens. Matter* **22**, 022201 (2010).
- ⁷⁷ A. V. Krukau, O. A. Vydrov, A. F. Izmaylov, and G. E. Scuseria, *J. Chem. Phys.* **125**, 224106 (2006).
- ⁷⁸ D. Yang, J. Lv, X. Zhao, Q. Xu, Y. Fu, Y. Zhan, A. Zunger, and L. Zhang, *Chemistry of Materials* **29**, 524 (2017).
- ⁷⁹ G. K. Madsen and D. J. Singh, *Comput. Phys. Commun.* **175**, 67 (2006).
- ⁸⁰ C. C. Stoumpos, C. D. Malliakas, and M. G. Kanatzidis, *Inorg. Chem.* **52**, 9019 (2013).
- ⁸¹ T. Baikie, Y. Fang, J. M. Kadro, M. Schreyer, F. Wei, S. G. Mhaisalkar, M. Graetzel, and T. J. White, *J. Mater. Chem. A* **1**, 5628 (2013).
- ⁸² W. S. Yang, J. H. Noh, N. J. Jeon, Y. C. Kim, S. Ryu, J. Seo, and S. I. Seok, *Science* **348**, 1234 (2015).
- ⁸³ H. Zhou, Q. Chen, G. Li, S. Luo, T.-b. Song, H.-S. Duan, Z. Hong, J. You, Y. Liu, and Y. Yang, *Science* **345**, 542 (2014).
- ⁸⁴ D. P. McMeekin, G. Sadoughi, W. Rehman, G. E. Eperon, M. Saliba, M. T. Hörantner, A. Haghighirad, N. Sakai, L. Korte, B. Rech, et al., *Science* **351**, 151 (2016).
- ⁸⁵ D. Bi, W. Tress, M. I. Dar, P. Gao, J. Luo, C. Renevier, K. Schenk, A. Abate, F. Giordano, J.-P. C. Baena, et al., *Sci. Adv.* **2**, e1501170 (2016).
- ⁸⁶ Y. Yamada, T. Nakamura, M. Endo, A. Wakamiya, and Y. Kanemitsu, *Appl. Phys. Express* **7**, 032302 (2014).
- ⁸⁷ H.-S. Kim, C.-R. Lee, J.-H. Im, K.-B. Lee, T. Moehl, A. Marchioro, S.-J. Moon, R. Humphry-Baker, J.-H. Yum, J. E. Moser, et al., *Sci. Rep.* **2**, 591 (2012).
- ⁸⁸ S. Pang, H. Hu, J. Zhang, S. Lv, Y. Yu, F. Wei, T. Qin, H. Xu, Z. Liu, and G. Cui, *Chem. Mater.* **26**, 1485 (2014).
- ⁸⁹ T. M. Koh, K. Fu, Y. Fang, S. Chen, T. C. Sum, N. Mathews, S. G. Mhaisalkar, P. P. Boix, and T. Baikie, *J. Phys. Chem. C* **118**, 16458 (2014).
- ⁹⁰ N. Pellet, P. Gao, G. Gregori, T.-Y. Yang, M. K. Nazeeruddin, J. Maier, and M. Grätzel, *Angew. Chem.-Int. Edit.* **53**, 3151 (2014).
- ⁹¹ J. Li and P. Rinke, *Phys. Rev. B* **94**, 045201 (2016).
- ⁹² A. Amat, E. Mosconi, E. Ronca, C. Quarti, P. Umari, M. K. Nazeeruddin, M. Grätzel, and F. De Angelis, *Nano Letters* **14**, 3608 (2014).
- ⁹³ A. Stroppa, D. Di Sante, P. Barone, M. Bokdam, G. Kresse, C. Franchini, M.-H. Whangbo, and S. Picozzi, *Nat. Commun.* **5**, 5900 (2014).
- ⁹⁴ M. Kepenekian, R. Robles, C. Katan, D. Saponi, L. Pedesseau, and J. Even, *ACS Nano* **9**, 11557 (2015).
- ⁹⁵ T. Etienne, E. Mosconi, and F. De Angelis, *J. Phys. Chem. Lett.* **7**, 1638 (2016).
- ⁹⁶ Y. Zhai, S. Baniya, C. Zhang, J. Li, P. Haney, C.-X. Sheng, E. Ehrenfreund, and Z. V. Vardeny, *Sci. Adv.* **3**, e1700704 (2017).
- ⁹⁷ M. Sebastian, J. A. Peters, C. C. Stoumpos, J. Im, S. S. Kostina, Z. Liu, M. G. Kanatzidis, A. J. Freeman, and B. W. Wessels, *Phys. Rev. B* **92**, 235210 (2015).
- ⁹⁸ X. Zhang, H. Lin, H. Huang, C. Reckmeier, Y. Zhang, W. C. H. Choy, and A. L. Rogach, *Nano Letters* **16**, 1415 (2016).
- ⁹⁹ D. Di Sante, P. Barone, R. Bertacco, and S. Picozzi, *Adv. Mater.* **25**, 509 (2013).
- ¹⁰⁰ L. Leppert, S. E. Reyes-Lillo, and J. B. Neaton, *J. Phys. Chem. Lett.* **7**, 3683 (2016).
- ¹⁰¹ W.-J. Yin, T. Shi, and Y. Yan, *Adv. Mater.* **26**, 4653 (2014).
- ¹⁰² J. Even, L. Pedesseau, and C. Katan, *J. Phys. Chem. C* **118**, 11566 (2014).
- ¹⁰³ H. Oga, A. Saeki, Y. Ogomi, S. Hayase, and S. Seki, *J. Am. Chem. Soc.* **136**, 13818 (2014-10-01).
- ¹⁰⁴ Q. Dong, Y. Fang, Y. Shao, P. Mulligan, J. Qiu, L. Cao, and J. Huang, *Science* **347**, 967 (2015).
- ¹⁰⁵ R. L. Milot, G. E. Eperon, H. J. Snaith, M. B. Johnston, and L. M. Herz, *Advanced Functional Materials* **25**, 6218 (2015).
- ¹⁰⁶ T. M. Brenner, D. A. Egger, A. M. Rappe, L. Kronik, G. Hodes, and D. Cahen, *J. Phys. Chem. Lett.* **6**, 4754 (2015).
- ¹⁰⁷ X.-Y. Zhu and V. Podzorov, *J. Phys. Chem. Lett.* **6**, 4758 (2015).
- ¹⁰⁸ B. Kang and K. Biswas, *Phys. Chem. Chem. Phys.* **19**, 27184 (2017).